Graphite Ablation in Combined Convective and Radiative Heating

ROY M. WAKEFIELD* AND DAVID L. PETERSON*
NASA Ames Research Center
Moffett Field, Calif.

Graphite ablation experimental results in the diffusion controlled oxidation and sublimation regimes are compared with results of an equilibrium chemistry, film coefficient ablation analysis. Mass transfer and energy transfer effects are considered. Tests were conducted in an arcjet facility at convective heating rates of 600–800 w/cm^2, radiative heating rates up to 2900 w/cm^2, with test specimen surface pressures of 0.06, 0.1, and 0.3 atm in an airstream. The experimental and analytical mass loss and surface temperature results agreed well when the carbon vapor thermodynamic properties from the JANAF tables are used in the analysis.

Nomenclature

B' = dimensionless mass injection rate, $(\rho v)_w/\rho_e U_e C$
C, C_0 = Stanton numbers with and without mass injection, respectively
c_p = specific heat
h_e = enthalpy of stream gas at boundary-layer edge
h_s = enthalpy of surface material
h_w = enthalpy of gas mixture adjacent to wall
k = thermal conductivity
$\dot{m}_s$ = surface mass loss rate
p_s = total model surface pressure
$\dot{q}$ = heating rate
R_n = nose radius
T_s = surface temperature
U_e = velocity at edge of boundary layer
v = gas velocity normal to surface
α = surface absorptance
ε = surface emittance
ρ = density of gas
σ = Stefan-Boltzmann constant

Subscripts

c = convection
cond = conduction
e = evaluated at boundary-layer edge
r = radiation
s = surface
w = adjacent to wall (surface)

Introduction

THERE is interest in graphite ablation performance for varied reasons. General ablation relations and procedures that may be applied to evaluate graphite ablation have been established,[1] but agreement of analytical and experimental results has not been demonstrated. However, the graphite-type materials are candidate ablators and have been used as comparison standards in ablation materials survey tests.[2] In planetary entry mission studies, analysis of heat shield requirements have been based on graphite-type ablators.[3,4] In addition investigations of specific aspects of graphite ablation have been performed.[5] The performance of graphite as determined from ablation theory is used in the analyses in all these applications. Also, the ablation mechanisms of graphite include important elements common to graphite and more complicated ablation materials (as shown in the general analysis of Ref. 1). The performance analysis of ablating graphite comprises mass-transfer and heat-transfer analysis. In the mass-transfer analysis, a controversy exists regarding the thermodynamic properties of the carbon gas system.[6,7] In the energy transfer, there has been little experimental verification of the analytical modeling. Also, it has not been demonstrated that the ablation chemistry approaches equilibrium sufficiently for application of an equilibrium analysis. Thus the present experimental results increase the reliability of heat shield evaluations for varied applications by advancing understanding of basic ablation mechanisms.

The objective of this work was to obtain experimental measurements of graphite mass transfer, especially in sublimation, and heat transfer for comparison with analytical results.

Description of Tests

The ablation experiments were performed in the Ames Advanced Entry Heating Simulator (Fig. 1), which is described in Ref. 8. This facility consists of independent convective and radiative heating systems. Convective heating is provided by an electric-arc heated, supersonic stream. The radiative heating system comprises an argon arc radiation source and arc-imaging mirror optics. In experiments the test specimen is positioned on the centerline of the convective stream, and at the location of the focused radiation. In the present tests the radiative heating rates ranged up to approximately 2900 w/cm^2, the convective heating rates were from 600 to 800 w/cm^2, and the test specimen surface pressures were from about 0.06–0.33 atm. The primary instruments employed in tests in this facility are steady-state and transient calorimeters, pressure probes, and a recording pyrometer. Descriptions of the critical calibration and measurement techniques for the heating rate and pyrometer instrumentation are presented in the appendix.

The graphite used in the present tests is a fine-grained nearly isotropic material (Union Carbide, Grade ATJ Graphite). Specific gravity of the graphite, based on measurements of three randomly selected samples, was 1.73 ± 0.09. The graphite test specimen (Fig. 2) was a hollow hemisphere-cylinder machined from bulk commercial material. A thin-wall test specimen was used to minimize material mass in the test region of the specimen, and thus shorten the time required to reach stable

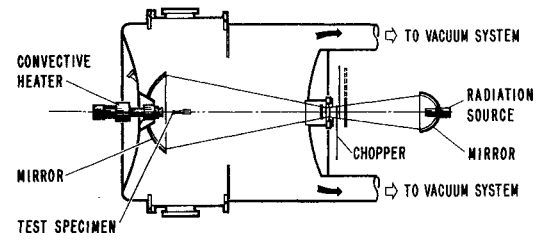

Fig. 1 Plan view of Advanced Entry Heating Simulator.

Presented as Paper 72-88 at the AIAA 10th Aerospace Sciences Meeting, San Diego, Calif., January 17-19, 1972; submitted February 3, 1972; revision received July 5, 1972.

Index categories: Material Ablation; Thermal Modeling and Experimental Thermal Simulation.

* Research Scientist.

Table 1 Experimental results from initial tests

p_s atm	$\dot{q}_c$ w/cm² (adjusted for blunting)	$\dot{q}_r$ w/cm²	$\dot{m}_s$ gm/cm²-sec	T_s °K	$\dot{m}_s\left(\frac{R_n}{p_s}\right)^{1/2}$ $\frac{\text{gm}}{\text{cm}^2\text{-sec}}\left(\frac{\text{cm}}{\text{atm}}\right)^{1/2}$
0.065	540	1500	0.0192	3510	0.091–0.100
0.12	670	0	0.0067	2520–2620	0.017
0.12	670–600	2150	0.0276	3650	0.069–0.077
0.12	670–575	2895	0.0485	3700	0.122–0.135
0.32	800	0	0.0117	2520–2700	0.018
0.32	800–730	1640	0.0239	3600	0.037–0.040
0.32	800–700	1970	0.0298	3630	0.046–0.052
0.32	800–750	2490	0.0408	3710	0.062–0.066
0.30	630	0	0.0099	2470–2610	0.016
0.30	630–600	820	0.0110	3000–3210	0.017

temperatures. In addition, a thin-wall specimen provided an experimental approach closely simulating the one-dimensional heat-transfer model of the analysis by minimizing the distance from the heated front surface and the radiation-cooled rear surface, relative to the radial extent of the uniformly heated region. In the stagnation region, the radiative heating distribution varied less than $\pm 10\%$ over a 0.6 cm radius,[8] and the convective heating on the hemisphere-nosed specimen varied approximately 10%[9] over the same area. During the test, the specimen was supported at the base by a threaded graphite member.

A nominally standardized test procedure was followed in obtaining data at each test condition. In a test run, preselected test conditions were established, and calorimeters, pressure probe, and ablation specimens (three or four) were automatically inserted sequentially into the test position. The actual test conditions, the ablation specimen surface temperatures, and test times were determined from test records; the ablation specimen stagnation point recessions were determined by direct postrun measurements. Recession measurements were plotted as a function of test specimen exposure time. The reported mass loss rates are the product of the slope of a linear fairing of such data and the material density. Representative test results are shown in Fig. 3 and the data for all tests are presented in Tables 1 and 2. The experimental uncertainty in the tabulated results is estimated as surface pressure $\pm 3\%$, convective heating rates $\pm 5\%$, radiative heating rates $\pm 10\%$, mass loss rates $\pm 10\%$, surface temperatures (Table 2 only) $\pm 3\%$.

The basis for the uncertainty in the heating rates and surface temperatures, and the reason for not giving an error value for the surface temperatures of Table 1, are discussed in the appendix. The heating rates for the test results given in Table 2 are not used in the analysis and are not presented. The uncertainty in the mass loss rates is based on comparison of results of separate test runs at identical conditions.

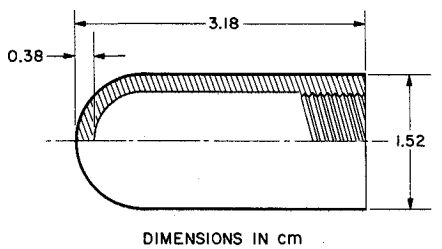

Fig. 2 Graphite ablation test specimen.

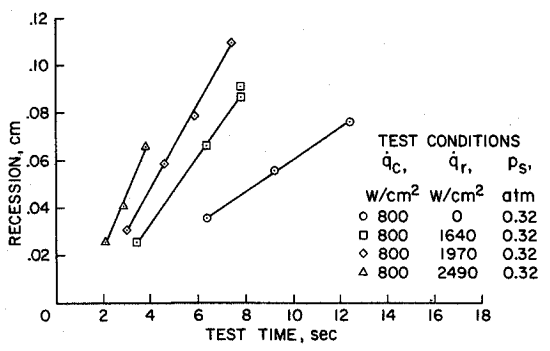

Fig. 3 Representative test results for ablation of ATJ graphite.

Analytical Method

The determination of ablation performance involves analysis of both heat and mass transfer effects, and includes important coupling relationships. The over-all objective of ablation analysis is to determine the ablation mass loss, or ablation flux, that results from specified conditions of convective and radiative heating. The analytical method used in this paper, which has been described frequently in ablation literature (Ref. 1, for example), is generally termed a "film coefficient approach." This analysis of heat and mass transfer implies unity Prandtl and Lewis numbers and equal diffusion coefficients for all chemical species in the boundary layer. In this analysis, an energy balance and a mass balance are performed on a control volume adjacent to the ablating surface.

The energy balance is the determination of the apportioning of the applied energy among the energy accommodation mechanisms. As sketched in Fig. 4, the applied convective heating (after reduction by mass transfer blockage) and radiative heating are accommodated at the ablating wall by chemical reactions, surface reradiation, and reflection, or conducted into the ablating material. The energy relation is

$$\rho_e U_e C(h_e - h_w) + \alpha \dot{q}_r - \dot{m}_s h_s = (\rho v)_w h_w + \varepsilon \sigma T_s^4 + \dot{q}_{\text{cond}}$$

Table 2 Experimental results from latter tests

p_s, atm	T_s, °K	$\dot{m}_s(R_n/p_s)^{1/2}$ $\frac{\text{gm}}{\text{cm}^2\text{-sec}}(\text{cm/atm})^{1/2}$
0.065	2550–2760	0.015
0.065	3170	0.020
0.065	3290	0.030
0.067	3390	0.039
0.068	3460	0.064–0.072
0.10	3320	0.024
0.11	3430	0.039
0.11	3480	0.050

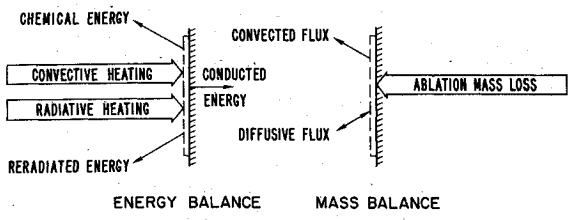

Fig. 4 Graphite ablation analysis.

This relation may be rearranged in terms of the sketched energy components by noting (from Ref. 10) that

$$(\rho v)_w = \dot{m}_s$$

$$\rho_e U_e C h_e + \alpha \dot{q}_r - \varepsilon\sigma T_s^4 - \dot{q}_{\text{cond}} = \dot{m}_s(h_w - h_s) + \rho_e U_e C h_w$$

The terms on the left side are the portion of the convective heating reaching the surface, absorbed radiative heating, reradiated energy, and energy conducted into the material, respectively. On the right side are the chemical energy terms that involve the enthalpy of the solid surface material or the enthalpy of the gas in the control volume as determined in the mass balance. A nominal value for the nonablating film coefficient, $\rho_e U_e C_0$ is 0.113 $(p_s/R_n)^{1/2}$ g/cm^2-sec, and in this paper the nonablating and ablating film coefficients are related by $C/C_0 = \ln(1.28B' + 1)/1.28B'$. The film coefficient and blockage relation are consistent with results of detailed boundary analyses[11] for ablation products from a graphite surface in an air stream.

The mass balance analysis treats the ablation material flux entering the control volume, and the diffusive and convected boundary-layer fluxes (Fig. 4). An equilibrium analysis of the control volume chemical reactions is made utilizing free-energy minimization techniques. As shown in Ref. 1 for a given chemical system, a specified surface pressure is sufficient to determine a unique temperature for a specified value of the dimensionless mass loss parameter B'. The surface mass loss parameter that will be used is $\dot{m}_s(R_n/p_s)^{1/2} = 0.113 \ln(1.28B' + 1)/1.28$. This parameter, within the constraints of the analysis, is a unique function of surface pressure and surface temperature for graphite ablating in an air boundary layer.

In the analytical results, 23 chemical species have been considered in the chemical reaction analysis. The gaseous carbon species are C_1 through C_{10}; the thermodynamic properties for the carbon molecules are from Refs. 12 and 13. Other chemical species of significance in the calculations are CO, CN, and N; the thermodynamic properties are also from Ref. 12.

Discussion of Results

A discussion of graphite ablation phenomena divides naturally into the areas of mass transfer, energy transfer, and the over-all performance involving the coupled effects of both energy and mass transfer. The mass-transfer analysis may be performed independently of the energy analysis, and thus is a convenient area to treat initially. In the following energy transfer analysis, the applied heating inputs are considered along with important chemical energy mechanisms based on results of a mass transfer analysis. The over-all performance of the ablator will then be considered to establish coherence of the energy and mass transfer analysis and to demonstrate the sufficiency and validity of the present analysis.

Mass Transfer

The results of tests of a graphite ablator that achieves surface temperatures of 3700° K are shown in Fig. 5 in the form of the surface mass loss parameter. There are three characteristic chemical reaction regimes of graphite ablation. At temperatures below about 3200° K, mass loss from a graphite surface at low surface pressures in an airstream is due to surface oxidation, and the mass transfer parameter is fairly constant over

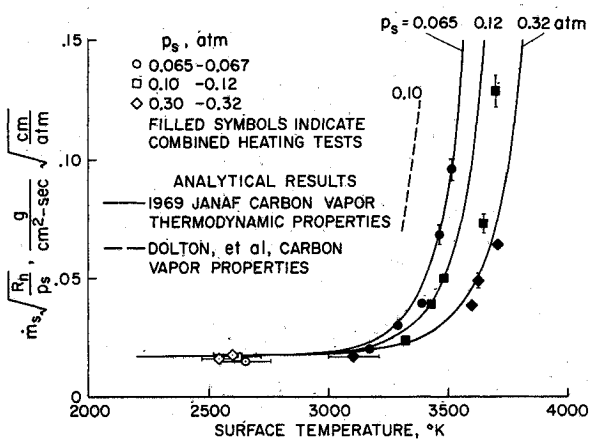

Fig. 5 Mass-transfer results for graphite in an airstream.

a wide temperature because the only reaction product is carbon monoxide. In effect, the stoichiometric ratios in the control volume are essentially constant, and the control volume mole fraction of CO is approximately 0.35. In the surface temperature range of approximately 3300°–3450° K (at the pressures of the present experiments), CN begins to appear as a reaction product (in the control volume gas equilibrium calculations) as the mass loss parameter increases with increasing temperature. The control volume mole fraction of CN becomes significant and reaches a maximum value of about 0.08 before decreasing again, the CO mole fraction decreases, and C_3 is also indicated in increasing mole fraction. At higher temperatures, surface sublimation occurs at a relatively constant temperature that is related to the surface pressure (More detailed discussion of mass transfer in graphite ablation is presented in Refs. 14 and 2.).

To demonstrate that the experimental environment simulated the analytical model, tests were made in the surface oxidation regime. The surface oxidation regime of graphite, which has been studied extensively and is noncontroversial, is indicated by values of the mass loss parameter of less than 0.02 in the analytical results of Fig. 5. Initially, tests that resulted in mass loss by surface combustion were performed in convective or in modest combined heating, and the results are shown in Fig. 5. Bars on the data points in the oxidation tests indicate the variation in surface temperature of the ablation test specimen during the period of constant rate, constant nose radius ablation. In the oxidation regime, the level of the mass loss parameter is of greater interest than a completely stable surface temperature. The test specimen exposure times were adjusted so that there was negligible nose blunting. The resulting unavoidable variation in the surface temperature is shown. Surface temperatures in the surface oxidation tests range from 2500° to 3100° K, and there is no discernible anomaly introduced by the radiative heating input indicated by the results in this chemical reaction regime. The surface oxidation results do show that the test stream, without or with radiative heating, provides a test environment that is compatible with the analytical model. The radiative heating, added in the sublimation experiments, ranged from approximately 1600–2900 w/cm^2. At the test pressures, surface reradiation is limited to about 1000 w/cm^2, and the graphite surface is forced into surface sublimation to absorb the additional applied heating. Therefore, the only change for the sublimation tests, in the combination of experimental and analytical modelling, is that chemical reactions are occurring in the sublimation regime.

The analysis of the test results must include consideration of 1) whether the chemical reactions in the experiments will proceed sufficiently close to equilibrium for the experimental results to lead to definitive conclusions when compared with an equilibrium analysis; and 2) whether sufficiently valid thermodynamic properties, for those chemical species in controversy such as the carbon gases, are available for application in analysis.

Consideration of the experimental results in each chemical

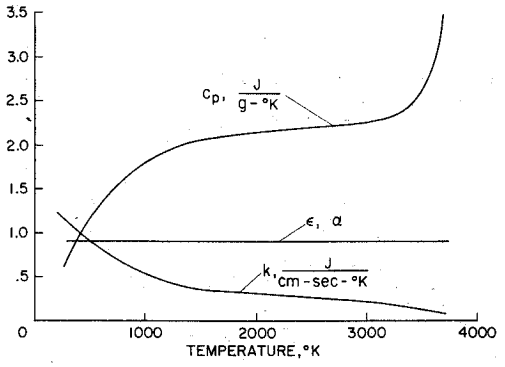

Fig. 6 Graphite properties used in analysis.

reaction regime will show a consistent analysis for the results in Fig. 5. In the surface oxidation regime previously discussed, the experimental mass loss levels could occur only if the CO forming reactions were near completion. This is firm evidence of at least one type of reaction approaching equilibrium. Reactions forming CN are similar to the oxidation reaction in that the reactants are a stream gas and surface material. Values of the mass transfer parameter above 0.02 include CN reactions, when the surface (or control volume) temperature is at the threshold of sublimation values. The experimental results at a surface pressure of 0.33 atm and temperatures above 3600° K include reactions in the CN formation regime. These data points are in reasonable accord with the analytical results, and indicate CN reactions and the onset of the carbon sublimation reactions. The sublimation regime, at a given pressure, is characterized by a variation in the surface mass loss parameter over a narrow range of temperature. Bars on the symbols in the sublimation data in Fig. 5 indicate the variation in the mass loss parameter due to nose radius changes during the period of constant rate, constant temperature ablation. The sublimation temperatures are of paramount interest, and nominal nose blunting was unavoidable in the experiments. After each test run, the nose radius of a test specimen was measured and the effective nose radius determined by methods of Ref. 15. In cases where the nose blunting was significant, the bars on the data symbols in Fig. 5 indicate the range of the effects of change from the initial 0.76 cm to the maximum effective nose radius. The measured and calculated sublimation results agree within measurement accuracy, at the test pressures.

There is no general agreement regarding carbon vapor thermodynamic properties (enthalpy and entropy functions), and the use of properties that are available produces significant variations in the analytical results. The analytical results presented in Fig. 5 were determined with carbon vapor thermodynamic properties of C_1 through C_5 obtained from the JANAF Thermochemical Tables,[12] and for C_6 through C_{10} from Duff and Bauer.[13] If the thermodynamic properties proposed in Ref. 6 are used in the analysis, the calculated sublimation temperatures are about 290° K lower (as shown by the dashed line in Fig. 5 for 0.1 atm) than the measured results. Obviously, the revised thermodynamic properties do not provide analytical results that are consistent with the experiment. There is the possibility that serious nonequilibrium effects may exist in the experiments, and that the revised thermodynamic properties may be correct for the carbon vapors. However, the following analysis of energy transfer will provide additional support for the equilibrium approach based on properties from Refs. 12 and 13.

Several preliminary conclusions may be reached from the preceding analysis. All the experimental results are considered to be in reasonable agreement with the analytical results, in view of the experimental accuracy of the data and the approximate nature of the analytical results. These results indicate that the most appropriate of the available thermodynamic properties for equilibrium ablation analysis are those from the JANAF tables (Ref. 12, augmented by Ref. 13). Reasonable simulation of the mass transfer experiment by the analytical modeling and equilibrium chemistry analysis is indicated by the results.

Energy Transfer

The basic ablation phenomena can be examined by an energy transfer analysis. Further, the energy balance is coupled to the details of mass transfer and serves to demonstrate the consistency of the analytical model with the experimental results. The energy analysis requires ablation material thermal properties, in addition to the film coefficient values and blockage relation used in mass transfer analysis. For high density isotropic graphite, experimentally determined thermal properties are available to temperatures above 3800° K.[16] The specific heat and thermal conductivity, which are temperature-dependent, and the surface emissivity used in the analysis are shown in Fig. 6.

A basis for illustrating surface energy transfer effects is shown by considering the relative significance of the various energy accommodation mechanisms. Two test cases, convective heating alone, and combined convective and radiative heating with a maximum of sublimation effects (both at a surface pressure of 0.12 atm) will be treated. Applied heating inputs are approximately 653 w/cm^2, for the convective heating case, and 3460 w/cm^2 (573 w/cm^2 convection and 2890 w/cm^2 radiation) in the combined heating case (The convective heating rates are adjusted for the nose blunting that had occurred in the test run.). A chart of the energy accommodation is shown in Fig. 7. Conduction and surface reradiation are major mechanisms in both cases. In the combined heating case, the chemical absorption is also important, because of the energy involved in the sublimation process. In both cases the convective blockage and reflection of applied radiation are relatively minor effects. Other test cases fall between these two extremes in terms of the relative importance of the major energy accommodation mechanisms.

The reradiated, conducted, and chemical energies in the surface energy balance all depend on the surface temperature; therefore the surface temperature is an indicator of the validity of the energy transfer analysis. A comparison of the experimental and analytical results for surface temperature is shown in Fig. 8. In the calculations, each ablation case was treated as step heating to a 0.36-cm thick graphite wall initially at 294° K. The calculation inputs were the measured values of convective and radiative heating rates and the surface pressure. Each calculation is thus a transient solution, with the graphite surface temperatures, temperature profiles, and mass loss rates varying with time. Both the calculated and experimental results shown are at the end of the exposure time for each test specimen. The combined heating points are indicated by solid symbols (The results for all the individual test specimens of the data points listed in Table 1 are shown.). The conduction in the experiment was matched to the one-dimensional model of the analysis by use of thin-wall test specimens. The applied heating

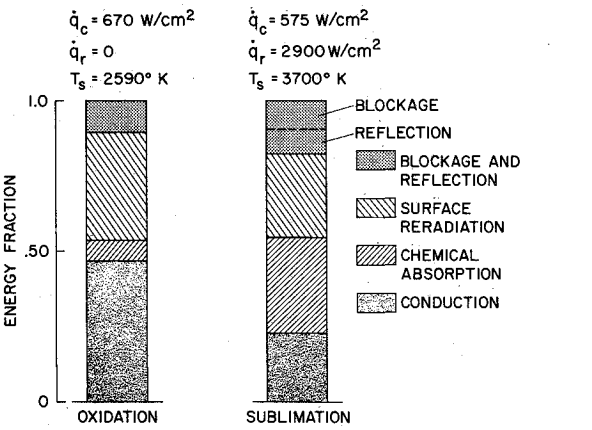

Fig. 7 Surface energy accommodation mechanisms in oxidation and sublimation regimes.

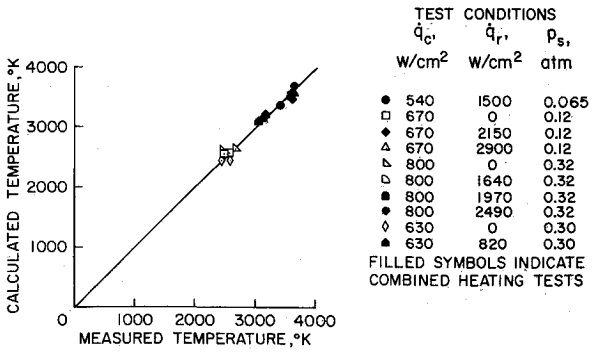

Fig. 8 Comparison of measured and calculated surface temperatures of ablating graphite.

rates were measured in the experiment, and used as inputs to calculate the analytical results. Therefore, energy accommodation in the surface reradiation and chemical reactions are essentially the effects illustrated. In all cases, the agreement between the measured and calculated values is excellent, and the results indicate acceptable modeling of the energy balance.

To evaluate ablator performance, the mass and energy analyses must be fully coupled; the over-all performance is then a final test of the analytical procedures. Components of the performance analysis, mass transfer, and energy transfer, have already been shown to be consistent with the experimental results. The object of the ablation analysis is to calculate the ablation mass loss and mass loss rates as a function of the applied heating conditions. A comparison of the measured and calculated mass loss results for the graphite ablation tests is shown in Fig. 9. (The calculated results are from the same computations used for the surface temperature comparison of Fig. 8.) Bars on the data points illustrate the range of variation in the calculated mass loss rates during the period of (experimental) constant rate ablation. The calculated and measured results all agree within a few percent.

As was indicated in the mass-transfer analysis, the use of the thermodynamic properties from Ref. 6 yields a performance analysis that does not agree with experiment. In the case with sublimation shown in Fig. 7, the calculated mass loss rate was 50% higher than measured, and the calculated surface temperature was 7% lower (225° K) than measured. The principal reasons for the increase in calculated mass loss rate are that the surface reradiation and the enthalpy of the gas in the control volume are reduced because of the lowered calculated surface temperature. Therefore, the calculated mass loss rate would increase to accommodate the applied heating by chemical reactions of lowered effectiveness.

The agreement obtained between the calculated and experimental ablation performance when the energy transfer and mass transfer analyses are coupled further supports the mass transfer analysis. In the ablation performance calculations, all the ablated material is removed only by chemical effects and must undergo the endothermic chemical reactions to accommodate all the applied heating. The film coefficient mass transfer analysis with thermodynamic properties from Refs. 12 and 13 provides analytical results that agree with the experimental results within measurement accuracy. The over-all success of the mutually consistent mass and energy transfer analyses is evidence that the approximations in the analysis are not significant in the analysis of ablator performance.

The loss of mass through mechanical erosion (the so-called particulate removal of solid graphite) was determined to be insignificant in these experiments. The two criteria advanced by others,[5] that is, photographic evidence and comparisons of experimental to calculated thermochemical mass loss rates, have been examined. Photographs of the nose of the ablating test specimens, taken at a 45° angle from the centerline with exposure times of 1/24000 sec, showed only occasional loss of particles. The photographic exposures were made at 1/500-sec intervals during runs of four test specimens each exposed for about seven seconds at the conditions of the 0.067 atm data point at a temperature of 3460° K and a mass-transfer parameter value of 0.064. Less than 20% of the individual photographic exposures showed evidence of particles, and such occurrences were limited to one or two particles from the entire nose of the ablation test specimen. By the other criterion used in Ref. 5, that of comparing the mass loss experimentally obtained with that calculated from thermochemical equilibrium analyses (mass transfer described herein), the data shown in Fig. 5 indicate no evidence of particulate mass loss. In addition, no recession occurred on the cylindrical body of the test specimen at the juncture of the nose radius, although the diameter at this high-temperature location of the test specimen would have been as affected as the stagnation point by any significant temperature-dependent particle loss such as discussed in Ref. 5. By measurements and postrun inspection, it was also determined that there was negligible material loss from the inside surfaces of the test specimens in any of the sublimation points at 0.12 and 0.32 atm pressure. All the additional tests would have clearly shown evidence of solid material loss, if a significant quantity of material were lost in particle form. Either negligible or no solid material loss was indicated in any case.

In the analysis of the present results, there is no method of directly showing that serious nonequilibrium effects are not present. Further, if some form of nonequilibrium is considered, analysis based on some other set of thermodynamic properties (such as the properties in Ref. 6) can probably be made of the present experimental results. However, a variety of nonequilibrium effects could conceivably occur and the result could be, but is not limited to, a shift in the temperature (as discussed in Ref. 6). A nonequilibrium analysis would have to include energy transfer analysis, as well as mass transfer considerations. This equilibrium analysis of both energy and mass transfer provides complete and consistent analysis of the present results. Nonequilibrium is not considered here because the departure from the equilibrium analysis considered herein is negligible.

Concluding Remarks

A comparison has been made of analytical and experimental results for graphite ablating in an airstream, using a general analysis with detailed ablation chemistry to evaluate the material performance. The graphite ablation performance was considered in both the diffusion limited combustion and in the sublimation regimes, and in convective or combined convective and radiative heating. A film coefficient analysis is used, with the coefficients and the blockage function based on detailed boundary-layer calculations. The graphite thermal conductivity and specific heat used in the analysis are measured values within the temperature range of interest. The principal conclusion is that the ablation performance of graphite is closely

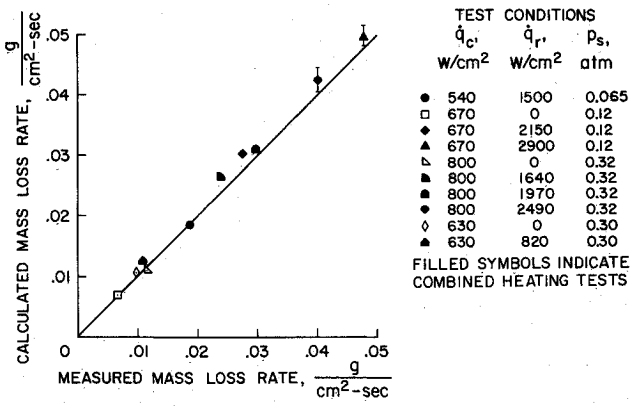

Fig. 9 Comparison of measured and calculated mass loss rate for ablating graphite.

modeled by a film coefficient, equilibrium chemistry approach using carbon vapor thermodynamic properties based on the JANAF thermochemical tables.

Appendix: Calibration and Measurement Techniques

The primary standards used for the heating rate measurements were transient ("slug") calorimeters. Initially, transient calorimeters with camphor-blackened surfaces were used to calibrate a steady-state calorimeter in radiative heating. For the calibration, the transient calorimeters were blackened with camphor soot to provide surface absorptance approaching unity. The surface of the steady-state calorimeter was not coated, but was a dull surface developed from repeated use in convective heating. The radiative heating rates were measured with a steady-state calorimeter, and the surface absorptance was presumed unchanged from calibration. In each test run, the convective heating rate measurements were made with 1.52 and 2.54 cm diam hemisphere-nosed transient calorimeters, and the 1.59 cm diam hemispherical-nosed steady-state calorimeter. The individual transient calorimeters that yielded several successive measurements inconsistent with the consensus of the other calorimeters were replaced with new calorimeters. The experimental uncertainty is less than $\pm 5\%$ for the convective heating rates, and considered less than $\pm 10\%$ for the radiative heating rates.

The test pyrometer, a commercial, monochromatic device with a narrow bandpass centered at 0.8 μ wavelength, was selected to provide the fast response required for radiative heating tests. In the initial testing phase the pyrometer calibration was compared with an optical pyrometer reading, using a tungsten strip lamp source. The true temperature of the tungsten strip was determined from the optical pyrometer readings, using values of tungsten emissivity from Ref. 17. The simultaneous readings of the test pyrometer, when corrected for the tungsten emissivity using values from Ref. 17 at 0.8 μ, agreed with the true strip temperature $\pm 2\%$. However, the maximum calibration temperatures attainable by this method are limited to 2800° K because tungsten emissivity values at 0.8 μ are not available at higher temperatures. The measurements of temperatures higher than 2800° K in the data in Table 1 must be regarded as based on an extrapolated pyrometer calibration for which the experimental accuracy cannot be assessed. For the pyrometer calibrations for the second block of tests (Table 2), a 3000° K blackbody source was available. An optical pyrometer was again used to determine the source temperature for comparison with the test pyrometer; no emissivity corrections were required because the source emissivity was unity. Further, during the tests a neutral density filter was inserted in the pyrometer view to limit radiation intensities on the pyrometer detector to the intensities of the calibration. During calibration of the pyrometer, the transmission through the filter and pyrometer viewing window was determined to be 45%. Use of the neutral density filter avoids assumption of pyrometer detector linearity at radiation intensity levels above calibrations temperatures, even though the instrument is used to measure higher temperatures. The resulting pyrometer calibration, even at the maximum test temperatures, was accurate within $\pm 2\%$. The pyrometer viewed the test specimen stagnation region at an angle of approximately 45° from the centerline, and the pyrometer signal was recorded continuously on an oscillograph or magnetic tape during ablation tests. In the radiative heating tests, the radiation chopper (Fig. 1) was used to periodically interrupt the incident radiation to eliminate reflected radiation effects in the pyrometer measurements. The surface temperature of an ablating test specimen was determined from the pyrometer record during the brief interval the incident radiation was blocked. (The portion of the pyrometer signal that resulted from reflected radiation was small after a test specimen reached high temperatures and the surface was roughened by ablation.) The adequacy of the chopping technique was checked by heating a test specimen in combined heating and extinguishing the radiation source in midrun. The surface temperature indicated during the "chopped" intervals just prior to terminating the radiation agreed with the measurements without radiation present. The resulting over-all uncertainty in the surface temperature results in Table 2 is estimated to be less than $\pm 3\%$. All pyrometric measurements were corrected for pyrometer-port window or filter and window absorption, and a test specimen surface emissivity of 0.90.

References

[1] Kendall, R. M., Rindal, R. A., and Bartlett, E. P., "Thermochemical Ablation," AIAA Paper 65-642, Monterey, Calif., 1965.

[2] Rindal, R. A., Kennedy, W. S., Powers, C. A., and Baker, D. L., "High Pressure Ablation Characterization of Graphite for Nose Tip Applications," *Graphite Materials for Advanced Re-Entry Vehicles*, edited by D. M. Forney, AFML TR-70-133, Pt. 1, Aug. 1970, Air Force Systems Command (Materials Lab.), Wright-Patterson Air Force Base, Ohio.

[3] Wakefield, R. M. and Lundell, J. H., "Ablative Heat Shields for Jupiter Entry Probes," AAS Paper 71-146, Seattle, Wash., 1971.

[4] Tauber, M. C. and Wakefield, R. M., "Heating Environment and Protection During Jupiter Entry," *Journal of Spacecraft and Rockets*, Vol. 8, No. 6, June 1971, pp. 630–636.

[5] Lundell, J. H. and Dickey, R. R., "Graphite Ablation at High Temperatures," *AIAA Journal*, Vol. 11, No. 2, Feb. 1973, pp. 216–222.

[6] Dolton, T. A., Goldstein, H. E., and Maurer, R. E., "Thermodynamic Performance of Carbon in Hyperthermal Environments," *AIAA Progress in Astronautics and Aeronautics: Thermal Design Principles of Spacecraft and Entry Bodies*, Vol. 21, edited by J. T. Bevans, Academic Press, New York, 1969, pp. 169–202.

[7] Kratsch, K. M., Martinez, M. R., Clayton, F. I., Greene, M. B., and Wuerer, J. E., "Graphite Ablation in High Pressure Environments," AIAA Paper 68-1153, Williamsburg, Va., 1968.

[8] Peterson, D. L., Gowen, F. E., and Richardson, C., "Design and Performance of a Combined Convective and Radiative Heating Facility," AIAA Paper 71-255, San Antonio, Texas, 1971.

[9] Kemp, N. H., Rose, P. H., and Detra, R. W., "Laminar Heat Transfer Around Blunt Bodies in Dissociated Air," *Journal of the Aerospace Sciences*., Vol. 26, No. 7, July 1959, p. 421–430.

[10] Moyer, C. B. and Rindal, R. A., "An Analysis of the Coupled Chemically Reacting Boundary Layer and Charring Ablator, Part 2: Finite Difference Solution for the In-Depth Response of Charring Materials Considering Surface Chemical and Energy Balances," CR-1061, June 1968, NASA.

[11] Bartlett, E. P. and Grose, R. D., "The Multicomponent Laminar Boundary Layer Over Graphite Sphere Cones: Solutions for Quasisteady Ablation and Application to Transient Reentry Trajectories," Rept. 68-35, May 1968, Aerotherm Corp., Mountain View, Calif.

[12] Stull, D. R. and Prophet, H., *JANAF Thermochemical Tables*, 2nd ed., Vol. 37, June 1971, National Standards Reference Data Series, National Bureau Standards (U.S.).

[13] Duff, R. E. and Bauer, S. H., "Equilibrium Composition of the C/H System at Elevated Temperatures," Rept. LA-2556, June 1961, Los Alamos Scientific Lab. of the Univ. of California, Los Alamos, N.Mex.

[14] Scala, S. M. and Gilbert, L. M., "Sublimation of Graphite at Hypersonic Speeds," *AIAA Journal*, Vol. 3, No. 9, Sept. 1965, pp. 1635–1644.

[15] Zoby, E. V. and Sullivan, E. M., "Effects of Corner Radius on Stagnation Point Velocity Gradients on Blunt Axisymmetric Bodies," TM X-1067, March 1965, NASA.

[16] Goldsmith, A., Waterman, T. E., and Hirschorn, H. J., *Handbook of Thermophysical Properties of Solid Materials*, Armour Research Foundation, Macmillan, New York, 1961.

[17] DeVos, J. C., "A New Determination of the Emissivity of Tungsten Ribbon," *Physica XX*, 1954, pp. 690–714.